

REPORT DOCUMENTATION PAGE

Form Approved
OMB No. 0704-0188

Public reporting burden for this collection of information is estimated to average 1 hour per response, including the time for reviewing instructions, searching existing data sources, gathering and maintaining the data needed, and completing and reviewing this collection of information. Send comments regarding this burden estimate or any other aspect of this collection of information, including suggestions for reducing this burden to Department of Defense, Washington Headquarters Services, Directorate for Information Operations and Reports (0704-0188), 1215 Jefferson Davis Highway, Suite 1204, Arlington, VA 22202-4302. Respondents should be aware that notwithstanding any other provision of law, no person shall be subject to any penalty for failing to comply with a collection of information if it does not display a currently valid OMB control number. PLEASE DO NOT RETURN YOUR FORM TO THE ABOVE ADDRESS.

1. REPORT DATE (DD-MM-YYYY)

2. REPORT TYPE
Technical Papers

3. DATES COVERED (From - To)

4. TITLE AND SUBTITLE

5a. CONTRACT NUMBER

5b. GRANT NUMBER

5c. PROGRAM ELEMENT NUMBER

6. AUTHOR(S)

5d. PROJECT NUMBER

2303

5e. TASK NUMBER

m2c8

5f. WORK UNIT NUMBER

7. PERFORMING ORGANIZATION NAME(S) AND ADDRESS(ES)

Air Force Research Laboratory (AFMC)
AFRL/PRS
5 Pollux Drive
Edwards AFB CA 93524-7048

8. PERFORMING ORGANIZATION
REPORT

9. SPONSORING / MONITORING AGENCY NAME(S) AND ADDRESS(ES)

Air Force Research Laboratory (AFMC)
AFRL/PRS
5 Pollux Drive
Edwards AFB CA 93524-7048

10. SPONSOR/MONITOR'S
ACRONYM(S)

11. SPONSOR/MONITOR'S
NUMBER(S)

12. DISTRIBUTION / AVAILABILITY STATEMENT

Approved for public release; distribution unlimited.

13. SUPPLEMENTARY NOTES

14. ABSTRACT

15. SUBJECT TERMS

16. SECURITY CLASSIFICATION OF:

17. LIMITATION
OF ABSTRACT

18. NUMBER
OF PAGES

19a. NAME OF RESPONSIBLE
PERSON

Leilani Richardson

a. REPORT

b. ABSTRACT

c. THIS PAGE

Unclassified

Unclassified

Unclassified

A

19b. TELEPHONE NUMBER

(include area code)

(661) 275-5015

Standard Form 298 (Rev. 8-98)
Prescribed by ANSI Std. Z39.18

122 025

C8

MEMORANDUM FOR PRS (Contractor/In-House Publication)

FROM: PROI (TI) (STINFO)

12 October 2000

SUBJECT: Authorization for Release of Technical Information, Control Number: **AFRL-PR-ED-TP-2000-193**
Christe, K.O. (ERC), Zhang, X. (USC), Sheehy, J. (PRSP), Bau, R. (USC), "Crystal Structure of $\text{ClF}_4^+\text{SbF}_6^-$, Normal Coordinate Analyses of ClF_4^+ , BrF_4^+ , IF_4^+ , SF_4 , SeF_4 , and TeF_4 , and Simple Method for Calculating the Effects of Fluorine Bridging on the Structure and Vibrational Spectra of Ions in a Strongly Interacting Ionic Solid"

Journal of the American Chemical Society

(Statement A)

1. This request has been reviewed by the Foreign Disclosure Office for: a.) appropriateness of distribution statement, b.) military/national critical technology, c.) export controls or distribution restrictions, d.) appropriateness for release to a foreign nation, and e.) technical sensitivity and/or economic sensitivity.

Comments: _____

Signature _____ Date _____

2. This request has been reviewed by the Public Affairs Office for: a.) appropriateness for public release and/or b) possible higher headquarters review

Comments: _____

Signature _____ Date _____

3. This request has been reviewed by the STINFO for: a.) changes if approved as amended, b.) appropriateness of distribution statement, c.) military/national critical technology, d.) economic sensitivity, e.) parallel review completed if required, and f.) format and completion of meeting clearance form if required

Comments: _____

Signature _____ Date _____

4. This request has been reviewed by PRS for: a.) technical accuracy, b.) appropriateness for audience, c.) appropriateness of distribution statement, d.) technical sensitivity and economic sensitivity, e.) military/national critical technology, and f.) data rights and patentability

Comments: _____

APPROVED/APPROVED AS AMENDED/DISAPPROVED

PHILIP A. KESSEL Date
Technical Advisor
Propulsion Science and Advanced Concepts Division

Cleared (PA) _____
Logged (PA) _____
Notified (PA) _____
Copied & Distributed (STINFO) _____
This original is for PA files

Crystal Structure of $\text{ClF}_4^+\text{SbF}_6^-$, Normal Coordinate Analyses of ClF_4^+ , BrF_4^+ , IF_4^+ , SF_4 , SeF_4 , and TeF_4 , and Simple Method for Calculating the Effects of Fluorine Bridging on the Structure and Vibrational Spectra of Ions in a Strongly Interacting Ionic Solid

Karl O. Christe,^{*†‡} Xiongzi Zhang,[‡] Jeffrey A. Sheehy,⁺ and Robert Bau[‡]

Propulsion Sciences and Advanced Concepts Division, Air Force Research Laboratory (AFRL/PRS), Edwards AFB, California 93524, and Loker Hydrocarbon Research Institute and Department of Chemistry, University of Southern California, Los Angeles, CA 90089

Abstract

The crystal structure of the 1:1 adduct $\text{ClF}_5\cdot\text{SbF}_5$ was determined and contains discrete ClF_4^+ and SbF_6^- ions. The ClF_4^+ cation has a pseudo-trigonal bipyramidal structure with two longer and more ionic axial bonds and two shorter and more covalent equatorial bonds. The third equatorial position is occupied by a sterically active free valence electron pair of chlorine. The coordination about the chlorine atom is completed by two longer fluorine contacts in the equatorial plane, resulting in the formation of infinite zigzag chains of alternating ClF_4^+ and *cis*-fluorine bridged SbF_6^- ions. Electronic structure calculations were carried out for the isoelectronic series ClF_4^+ , BrF_4^+ , IF_4^+ and SF_4 , SeF_4 , TeF_4 at the B3LYP, MP2 and CCSD(T) levels of theory and used to revise the previous vibrational assignments and force fields. The discrepancies between the vibrational spectra observed for ClF_4^+ in $\text{ClF}_4^+\text{SbF}_6^-$ and those calculated for free ClF_4^+ are largely due to the fluorine bridging that compresses the equatorial F-Cl-F bond angle and increases the barrier towards equatorial-axial fluorine exchange by the Berry mechanism. A computationally simple model, involving ClF_4^+ and two fluorine bridged HF molecules at a fixed distance as additional equatorial ligands, was used to simulate the

bridging in the infinite chain structure and greatly improved the fit between observed and calculated spectra.

Introduction

Binary halogen fluorides and their ions are ideally suited for studying molecular structures and bonding.¹⁻³ They cover a wide range of oxidation states from +I to +VII and coordination numbers from one to eight, including many examples of hypervalent compounds.⁴ The following binary chlorine fluorides are known: ClF, ClF₃ and ClF₅;⁵ they are amphoteric and, with strong Lewis acids, they can form adducts containing the Cl₂F⁺,⁶⁻⁸ ClF₂⁺,⁹⁻²⁰ and ClF₄⁺²¹⁻²² cations, respectively. Crystal structures, however, are known only for the ClF₂⁺ salts.¹⁵⁻²⁰ Although these structures confirm the predominantly ionic nature of the adducts, strong interactions between the ClF₂⁺ cations and the anions were observed which result in infinite chains, distort some of the ions and complicate the vibrational spectra. Chlorine pentafluoride also forms adducts with AsF₅ and SbF₅, but only the ClF₅·SbF₅ complex is stable at room temperature.^{21,22} Based on their vibrational spectra, a predominantly ionic structure was proposed^{22,23} for the ClF₅·MF₅ adducts with ClF₄⁺ most likely possessing a pseudo-trigonal bipyramidal structure of C_{2v} symmetry, similar to those found for isoelectronic SF₄²⁴ and the heavier halogen analogues BrF₄⁺²⁵ and IF₄⁺.^{26, 27} In view of the significant cation-anion interactions found for the related ClF₂⁺ salts,¹⁵⁻²⁰ it was desirable to confirm by x-ray diffraction the postulated C_{2v} structure for ClF₄⁺, to obtain its exact geometry, and to determine the nature and influence of any interionic interactions. Electronic structure calculations were used to critically examine the previously reported crystal structures for BrF₄⁺²⁵ and IF₄⁺,^{26, 27} and the vibrational spectra of the ClF₄⁺, BrF₄⁺, and IF₄⁺ cations^{22, 28} and of the isoelectronic SF₄, SeF₄ and

TeF₄ molecules. Furthermore, we outline a computationally simple method for modeling the influence of interionic fluorine bridging on the structure and vibrational spectra of the free ions.

Experimental

Crystal Structure Determination. A sample of ClF₄⁺SbF₆⁻ was prepared as previously described,^{21, 22} and single crystals were grown from solutions in anhydrous HF. Due to the moisture sensitivity of the crystals, a suitable crystal was selected and mounted with a drop of perfluoroether oil under a flow of cold dry nitrogen. The diffraction data were collected at -100 °C, using a Siemens/Nicolet/Syntex P21 diffractometer with MoK α radiation. The structure was solved by standard heavy-atom methods. The coordinates of the antimony and chlorine atoms were found from direct methods, and the atomic positions of the remaining fluorine atoms were revealed by subsequent difference-Fourier maps.²⁹

Theoretical Calculations. Theoretical calculations were carried out on IBM RS/6000 work stations using the Gaussian 98³⁰ and ACES II³¹ program systems and the density functional B3LYP³² and the correlated MP2³³ and single-and double-excitation coupled cluster methods,³⁴ including a non-iterative treatment of connected triple excitations.³⁵

It was desirable to perform the calculations for SF₄, ClF₄⁺, SeF₄, BrF₄⁺, TeF₄, and IF₄⁺ by consistent methods. However, they involve atoms from the second, third, and fourth rows of the periodic table and it was not clear whether a single type of atomic basis sets could be found that would give accurate results for all six compounds. Whereas there are many choices of high-quality basis sets for second- and third-row elements, the choices available for tellurium and iodine are far fewer and generally lower in quality. Consequently, several different basis sets were examined, most of which involved the use of effective-core potentials for the inner-shell electrons on the central atoms. The criteria used for determining the relative suitability of the

basis sets for the present purposes was how well the experimentally observed vibrational spectra of SF₄ and SeF₄ was reproduced by the calculations. These molecules were chosen for the basis-set study because excellent experimental data are available for a comparison with the calculated frequencies and because there are many basis set choices for sulfur and selenium. Ultimately, it was found that the best results were obtained with the so-called DFT/DZVP all-electron basis sets,^{36,37} supplemented with one *f* function taken from either the cc-pVTZ basis sets of Woon and Dunning³⁸ (exponents: S = 0.557, Cl = 0.706, Se = 0.462, Br = 0.552) or the polarization functions of Ahlrichs³⁹ (exponents: Te = 0.474, I = 0.486) on the heavy atoms, and the 6-311+G(2d) basis sets of Pople⁴⁰ on fluorine. The calculated Hessian matrices (second derivatives of the energy with respect to Cartesian coordinates) were converted to symmetry-adapted internal coordinates for subsequent normal coordinate analyses using the program systems GAMESS⁴¹ and Bmtrx.⁴²

Results and Discussion

Crystal Structure of ClF₄⁺SbF₆⁻. ClF₄⁺SbF₆⁻ crystallizes in the orthorhombic space group Pbcm with the unit cell parameters given in Table 1. One hemisphere of data (3645 reflections) were collected at -100°C, merged to give one unique octant of data (880 reflections), and refined to a final agreement factor of R = 2.3 % for 854 reflections having I > 2σ(I). The crystal and structure refinement data, atomic coordinates and isotropic displacement parameters, and selected bond distances and angles are summarized in Tables 1-3, respectively. The structures of the ClF₄⁺ and SbF₆⁻ ions and the numbering scheme are shown in Figure 1, while the packing diagram and the interionic fluorine bridges are depicted in Figures 2 and 3, respectively.

As can be seen from Figures 1 and 2, the structure of the $\text{ClF}_5 \cdot \text{SbF}_5$ adduct is predominantly ionic consisting of discrete ClF_4^+ cations and SbF_6^- anions in a simple packing arrangement. The structure of the ClF_4^+ cation is best described as a trigonal bipyramid in which the four fluorine ligands occupy the two axial and two of the equatorial positions, while a sterically active free valence electron pair fills the third equatorial position.

The coordination in the equatorial plane is completed by two fluorine bridges with two different SbF_6^- anions, resulting in infinite zigzag chains along the *a*-axis (see Figure 3). The two interionic fluorine bridges formed by each SbF_6^- anion are *cis* with respect to each other and distort the SbF_6^- octahedron from O_h to C_{2v} symmetry. The Cl-F bond lengths of the two fluorine bridges, measuring 2.41 and 2.43 Å, respectively, are comparable to those of 2.23-2.43 Å found for similar ClF_2^+ salts,¹⁵⁻²⁰ and are significantly shorter than the Cl-F van der Waals distance of 3.15 Å.⁴³ The two equatorial and the two bridging fluorines and the chlorine atoms of ClF_4^+ are perfectly planar, as shown by the sum of their bond angles of 360.0 ° (see Table 3).

The geometry of ClF_4^+ , given in Table 3, is in accord with the VSEPR model of molecular geometry.⁴⁴ In an AX_4E -type species, such as ClF_4^+ , the crowding of the axial positions results in longer and more ionic axial bonds, while the more repulsive electron pair domain⁴⁵ of the equatorial free valence electron pair E causes compressions of the equatorial F-Cl-F angle from the ideal 120 to 103 ° and of the axial F-Cl-F angle from 180 to 174 °.

Structure Calculations for Free Gaseous ClF_4^+ , BrF_4^+ , IF_4^+ , and Isoelectronic SF_4 , SeF_4 , TeF_4 . Since the geometries and vibrational frequencies of SF_4 ^{24, 28} and SeF_4 ⁴⁶ are well known, these molecules were used to evaluate the quality of different basis sets at the B3LYP,³² MP2,³³ and CCSD(T)^{34, 35} levels of theory, with the DFT-DZVP basis^{36, 37} giving the best results. As can be seen from Tables 4 and 5, the MP2 and CCSD(T) calculations gave almost identical

results. The density functional B3LYP method duplicated best the observed bond angles, but slightly overestimated the bond lengths.

The observed and calculated geometries of ClF_4^+ are summarized in Table 6. Scaling the calculated Cl-F bond lengths with correction factors derived from the SF_4 data of Table 4, gives for free ClF_4^+ the predicted values shown in Table 6. The major discrepancies between these values and the ones, observed for ClF_4^+ in solid $\text{ClF}_4^+\text{SbF}_6^-$ are the compression of the equatorial angle by about 4° and an increase in the difference between the axial and the equatorial bond lengths by about 2.3 pm in $\text{ClF}_4^+\text{SbF}_6^-$. These changes can be attributed to the influence of the two equatorial fluorine bridges from two neighboring SbF_6^- anions. This conclusion is supported by model calculations for the bridged ClF_4^+ cation (see below).

The minimum energy structure of ClF_4^+ had been disputed in several previous publications. Thus, Ungemach and Schaefer predicted, based on SCF calculations with minimum and double zeta basis sets, that ClF_4^+ should be square-pyramidal.⁴⁷ In a note added in proof, however, they state that the inclusion of d functions resulted in a minimum energy structure of C_{2v} symmetry with $r \text{ Cl-F}_{\text{ax}} = 1.63 \text{ \AA}$, $r \text{ Cl-F}_{\text{eq}} = 1.57 \text{ \AA}$, $\angle \text{F}_{\text{ax}}\text{-Cl-F}_{\text{ax}} = 169.6^\circ$, and $\angle \text{F}_{\text{eq}}\text{-Cl-F}_{\text{eq}} = 109.7^\circ$. This finding was confirmed by So.⁴⁸ However, he surprisingly found that the axial bond (1.570 \AA) was shorter than the equatorial one (1.632 \AA) and his $\text{F}_{\text{eq}}\text{-Cl-F}_{\text{eq}}$ bond angle of 117.42° was also very different from that given by Ungemach and Schaefer. The C_{2v} geometry given by Ungemach and Schaefer was confirmed by several subsequent studies.⁴⁹⁻⁵² It was also shown⁴⁹ that at the RHF/DZP level the energy difference between the minimum energy C_{2v} structure and the square-pyramidal C_{4v} structure, which represents the transition state for the equatorial-axial ligand exchange by the Berry mechanism, is only $6.7 \text{ kcal mol}^{-1}$, while a square-planar D_{4h} structure was found to lie 59.5 kcal/mol above the C_{2v} structure.⁴⁹ Surprisingly,

however, the same study⁴⁹ found that at the MP2/DZP level the D_{4h} structure becomes energetically favored over the C_{2v} structure by 16.2 kcal/mol.

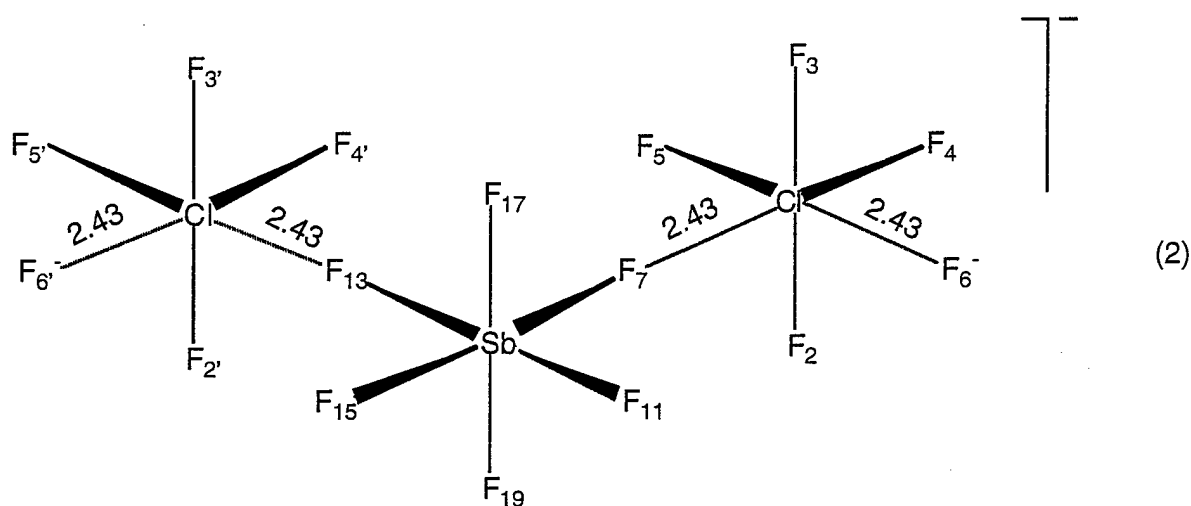
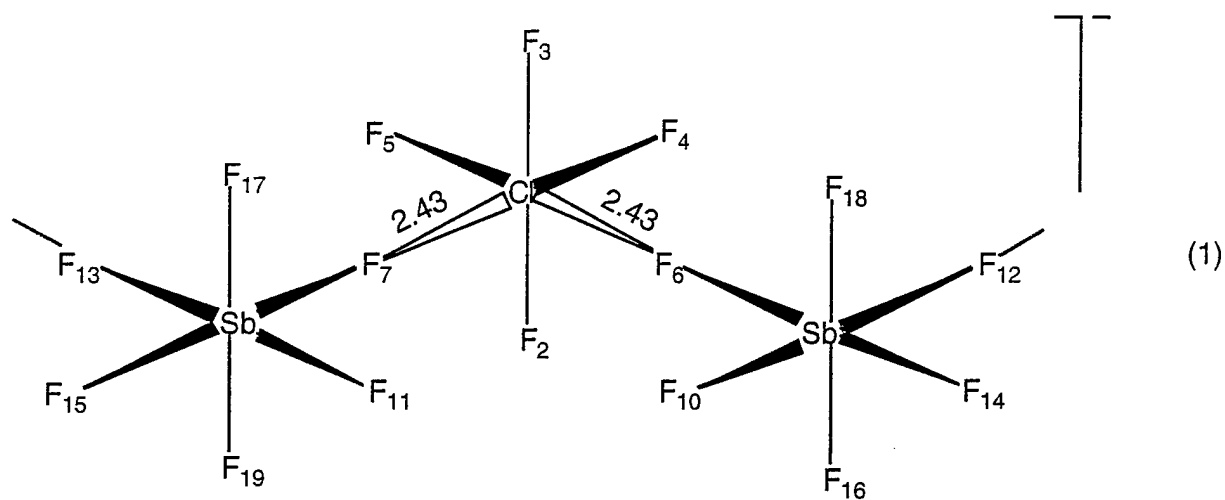
In our calculations, it was found that the C_{2v} structure was the minimum energy structure at the B3LYP, MP2 and CCSD(T) levels of theory with all the basis sets used. Duplication of previous computations showed that the omission of d-functions from basis sets indeed results in a square-pyramidal C_{4v} structure being the minimum. This is not surprising in view of the small energy difference of ~7kcal/mol between the C_{2v} and C_{4v} structures. However, the big change of 75.7 kcal/mol, reported⁴⁹ for the difference between the C_{2v} and D_{4h} structures on going from the RHF to the MP2 level could not be confirmed.

Table 7 gives a comparison between the observed and calculated structures of BrF_4^+ and IF_4^+ . For IF_4^+ , the deviations between the observed and calculated values agree with those noted for ClF_4^+ , but are more pronounced due to increased fluorine bridging. For BrF_4^+ , however, the observed bond lengths are much too long and also the axial bond angle is too big. These large deviations, together with the extremely large uncertainties in the crystal structure of $BrF_4^+Sb_2F_{11}^-$,²⁵ demonstrate the need for a redetermination of its crystal structure.

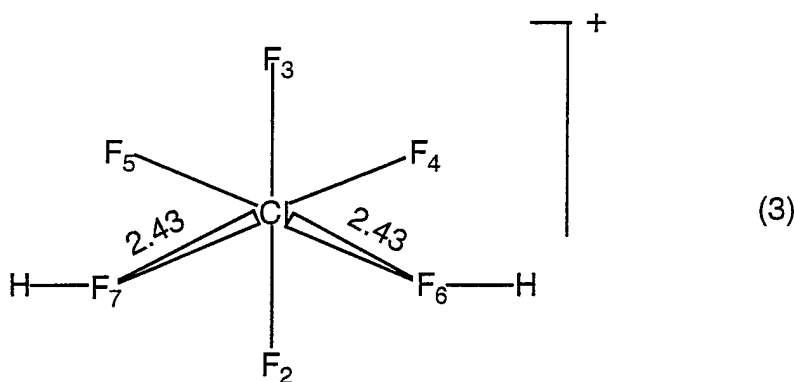
Structure Calculations for Fluorine Bridged ClF_4^+ in Solid $ClF_4^+SbF_6^-$. In many predominately ionic structures, consisting of coordinationwise unsaturated cations and saturated fluoro- or oxofluoro-anions, strong fluorine bridging is observed between the anions and cations. These fluorine bridges fill empty coordination sites of the cation and, at the same time, lower the symmetry of the anions. These effects profoundly influence the vibrational spectra of these compounds. They give rise to additional bands in the anion spectra due to the symmetry lowering from O_h to C_{2v} and create new vibrations due to the bridge bonds. Although the existence of these bridges has been well established through crystal structure studies, their influence on the

vibrational spectra has previously not been analyzed in sufficient detail and as a result, the vibrational assignments of the bridging modes have in most cases either been ignored or been poor guesses. This is not surprising because the cations generally form multiple fluorine bridges with different partners, thus resulting in difficult to analyze infinite chains. To circumvent this problem, most previous investigators have limited their analyses to symmetry lowering of the individual ions, followed by a factor group analysis. Whereas this approach is not unreasonable for the anions, because their coordination number remains the same and their geometry does not change dramatically, it accounts neither for the structural changes in the cation nor for the newly generated bridging modes.

One possible approach to duplicate the ClF_4^+ and SbF_6^- environments in the infinite zigzag chain involves the calculation of the trinuclear segments (1) and (2), using the observed Cl---F bridge distances as the only constraints and forcing the Sb-F₆, Sb-F₇, Sb-F₁₂ and Sb-F₁₃ distances to be equal, while the remaining parameters are optimized. This approach, however, still presents the following major problems. (i) Charge neutralization and chain termination become issues. In structure (1), the ClF_4^+ cation effectively becomes a polyanion; in structure (2), two F⁻ ions, F₆⁻ and F₆⁻, must be added to maintain the overall negative charge and the correct coordination around the chlorine atoms, but result in computationally unstable configurations that want to loose fluoride ions. (ii) Even with density functional methods and limited basis sets, the required computational effort is still large, and a vibrational analysis is complicated.



These problems were overcome in the following manner. Replacement of the two terminal SbF_6^- anions in (1) by neutral hydrogen fluoride molecules (3) maintains the positive charge of ClF_4^+ and greatly simplifies the calculation, while simulating well the two covalently bound, bridging fluorine ligands which were again constrained to the observed Cl-F bond distance of 2.43 Å.



In Table 8, the geometries calculated for $\text{ClF}_4^+ \cdot 2\text{HF}$ and free ClF_4^+ at the B3LYP/B4 level are compared to that observed for ClF_4^+ in $\text{ClF}_4^+ \text{SbF}_6^-$. As can be seen, the equatorial ClF_2 bond angle in $\text{ClF}_4^+ \cdot 2\text{HF}$ decreases strongly from free ClF_4^+ and the axial bond length increases, as expected for an increased ligand crowding in the equatorial plane due to the fluorine bridges. Furthermore, the bond length difference between equatorial and axial bonds increases from free ClF_4^+ to $\text{ClF}_4^+ \cdot 2\text{HF}$. All these changes are in the same direction, as observed for ClF_4^+ in $\text{ClF}_4^+ \text{SbF}_6^-$ and confirm that the discrepancies between the calculated geometry of free ClF_4^+ and the observed geometry of ClF_4^+ in solid $\text{ClF}_4^+ \text{SbF}_6^-$ are mainly due to fluorine bridge bonds and not to computational shortcomings.

A comparison of the calculated geometries of $[\text{SbF}_6-\text{ClF}_4-\text{SbF}_6]^-$ and free ClF_4^+ shows that the more rigorous treatment of doubly bridged ClF_4^+ as a trinuclear segment results in similar, although more pronounced trends. Thus, on going from free ClF_4^+ to $[\text{SbF}_6-\text{ClF}_4-\text{SbF}_6]^-$, $r(\text{ClFax})$, $r(\text{ClFeq})$ and $\angle(\text{FaxClFax})$ increased by 4.5 pm, 2.7 pm, and 1.1 °, respectively, while $\angle(\text{FeqClFeq})$ was compressed by 12.1 °. It therefore appears that the simplified model with HF bridging groups approximates the binding in $\text{ClF}_4 \text{SbF}_6$ better than the more elaborate trinuclear model.

Modeling the SbF_6^- distortion was simpler. The only constraint imposed on SbF_6^- was forcing the two equatorial Sb-F bonds, that are involved in the cis-fluorine bridging, to be 3 pm

longer than the two axial Sb-F bonds (the same amount as that observed in the crystal structure) and allowing the rest of the structure to maximize. The resulting structure is compared in Figure 4 to that observed for the crystal structure of ClF_4SbF_6 . The calculated structure exhibits angle changes, similar to but less pronounced than those observed for SbF_6^- in ClF_4SbF_6 . This can be attributed to the fact that in the calculated structure the Sb-F bonds *trans* to the fluorine bridges also become somewhat longer (*trans*-effect) and therefore, the angle deviations from 90° become smaller.

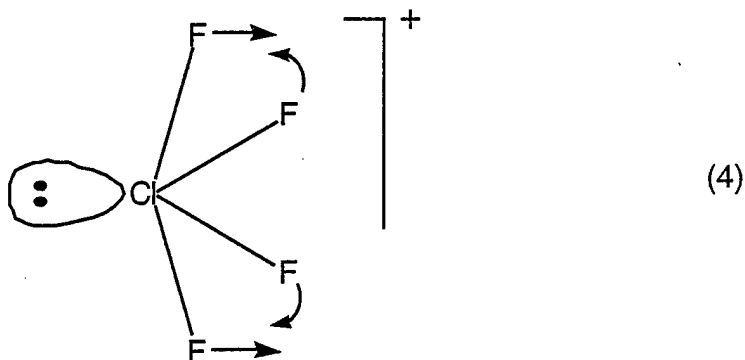
Vibrational Spectra

SF_4 . The observed and unscaled and scaled calculated vibrational spectra of SF_4 are listed in Table 9. The scaled B3LYP, MP2 and CCSD(T) frequencies fit about equally well, but the MP2 and CCSD(T) sets require less scaling.

The assignment of the vibrational spectra of SF_4 based on experimental data alone had been a most difficult and frustrating task and required at least 13 publications from several different laboratories.²⁸ In spite of all this previous work, our present study reveals that even in the most recent reassignment²⁸ there are still two errors. The infrared inactive Raman band observed at 475 cm^{-1} must be $\nu_5(\text{A}_2)$; and the infrared inactive $\nu_7(\text{B}_1)$ Raman band should occur at about 540 cm^{-1} and is apparently hidden by the two very intense Raman bands, $\nu_2(\text{A}_1)$ and $\nu_3(\text{A}_1)$ at 558 and 532 cm^{-1} , respectively. This reassignment results in an excellent fit between observed and calculated spectra, particularly if it is kept in mind that no anharmonicity corrections have been applied to the observed frequencies.

ClF_4^+ . Table 10 compares the vibrational frequencies calculated for free gaseous ClF_4^+ to those observed for solid $\text{ClF}_4^+\text{SbF}_6^-$. As expected, the agreement is not as good as for isoelectronic SF_4

where gas phase values were compared. However, the agreement is still very satisfactory and shows that the previously proposed²² assignments are correct. As for SF₄, the MP2 set gives the best frequency fit and the CCSD(T) set requires the least scaling. The agreement between the observed and the calculated MP2 values is better than 16 cm⁻¹ for all modes, except for $\nu_4(A_1)$ where the discrepancy of 69 cm⁻¹ is huge. This mode represents the antisymmetric combination of the axial and the equatorial scissoring motions (4) and is responsible for the inversion of the



axial and the equatorial ligands by the Berry pseudo-rotation mechanism.⁵⁴ As was pointed out already above and is also transparent from structure (1), the two equatorial fluorine bridges impede these motions and thereby increase the frequency of this mode and raise the barrier to the equatorial-axial ligand exchange in the solid.

The influence of the fluorine bridges in solid ClF₄⁺SbF₆⁻ on the vibrational frequencies of ClF₄⁺ was modeled, as described above for the geometries, at the B3LYP level with two bridging HF ligands. The results are summarized in Table 11 and show that the large discrepancy of 85 cm⁻¹ between the calculated frequency of ν_4 for free ClF₄⁺ and the observed one in ClF₄⁺SbF₆⁻ is indeed due to the fluorine bridging. For the bridged ClF₄⁺•2HF model, the discrepancy between the calculated and the observed frequencies of ν_4 shrinks to 13 cm⁻¹ and the fit of the remaining 8 frequencies was also greatly improved by 46 cm⁻¹. This result demonstrates that typical fluorine bridges, as encountered in many main group fluoride salts, cannot be ignored in a thorough

analysis, and that our simple model of using HF to replace large counter-ions and infinite chains is well suited for simulating the observed frequencies.

As pointed out above, most previous analysis had failed to correctly identify and assign the fluorine bridging modes in the infinite-chain, fluorine-bridged salts. Table 12 summarizes the results from our normal coordinate analysis of $\text{ClF}_4^+ \cdot 2\text{HF}$. As a nine-atomic species, it has 21 normal modes. Of these, 6 are associated with hydrogen motions (see footnote a) of Table 12) and are of little interest for our analysis, because hydrogen has been used only as a simulant for an SbF_5 group and the Sb-F modes are already included in the analysis of the (C_{2v}) SbF_6^- ion. It should be noted that the two hydrogen rocking modes have imaginary frequencies because constraining the Cl-F bridge bond length to the observed value resulted in a maximized geometry which is not a global minimum. The remaining 15 modes can be separated into nine fundamentals for ClF_4^+ (see Table 11) and six fundamentals for the fluorine bridges (see Table 12). The six fundamentals for the fluorine bridge modes are highly characteristic, except for the symmetric $\text{ClF}_{2\text{BR}}$ mode, $\nu_1'(A_1)$, which strongly couples with the Berry mode, $\nu_4(A_1)$, of ClF_4^+ (see footnote c of Table 11), due to their similar motions and frequencies. These mixings of the S3 and S4 symmetry coordinates of ClF_4^+ and of S4 of ClF_4^+ with S1' of fluorine bridged ClF_4^+ account for most of the difficulties encountered with attempts to fit the observed vibrational spectra with less rigorous analyses. Inspection of Tables 11 and 12 demonstrates that the bridging modes in $\text{ClF}_4^+ \text{SbF}_6^-$ occur below 230 cm^{-1} and, therefore, interfere only with the lowest frequency mode of ClF_4^+ . Since most of the bridging modes of solid $\text{ClF}_4^+ \text{SbF}_6^-$ occur in the range of the lattice modes, reliable observation and analysis of these modes are presently not possible.

SeF₄. Table 13 shows a comparison of the observed and calculated vibrational frequencies of free gaseous SeF₄. The listed observed frequencies are the gas phase values,^{55,56} except for that of ν_9 which was observed only as a very weak and broad band.⁵⁵ For this mode the averaged frequency of the molecule isolated in different matrices⁵⁵ was used. As in the case of gaseous SeF₄ (Table 9), the agreement between observed and calculated frequencies is excellent and, for the MP2 set, the scaling factors are also close to unity. These results lend strong support to our revised assignments given in Table 13. Of the previous assignments, only those given by Alexander and Beattie for 6 of the modes,⁵⁶ are correct. In the paper by Ramaswamy,⁵⁷ seven of the nine fundamentals were assigned incorrectly; in the study by Adams and Downs,⁵⁵ six fundamentals were assigned correctly, two incorrectly and one was missing; and in the most recent study by Seppelt of SeF₄ in CH₃F solution,⁵⁸ only four of the nine fundamentals were assigned correctly, and the latter assignments unfortunately have found their way into recent compilations, such as the book by Nakamoto.⁵⁹

TeF₄. The observed and calculated vibrational frequencies of TeF₄ are compared in Table 13. Since TeF₄ is polymeric at room temperature,⁶⁰ the frequencies of matrix isolated TeF₄⁵⁵ were used as the experimental values. The agreement between observed and calculated frequencies and infrared intensities is again very good and the scaling factors are similar to those used for SeF₄. Our results confirm the experimental frequencies, but show that the previous assignments⁵⁵ for $\nu_3(A_1)$ and $\nu_7(B_1)$ must be reversed.

BrF₄⁺ and IF₄⁺. The calculated vibrational frequencies for free gaseous BrF₄⁺ and IF₄⁺ are summarized in Table 14. Only partial experimental values are given for BrF₄⁺ and no values are given for IF₄⁺ because the reported spectra for these two cations are incomplete, their crystal structures are poorly determined, and fluorine bridging is expected to become more pronounced

with increasing atomic weights of the halogen central atoms. Clearly, both cations should be thoroughly reinvestigated.

C_{2v} Distorted SbF_6^- . To judge the influence of fluorine bridging on the vibrational spectra of SbF_6^- , the spectra of octahedral SbF_6^- and of C_{2v} distorted SbF_6^- were calculated at the B3LYP level. For (O_h) SbF_6^- , r was found to be 1.923 Å, and for (C_{2v}) SbF_6^- the geometry given in Figure 4b was used. The calculated vibrational spectra are summarized in Table 15 and show that even relatively small distortions of about 0.15 ° for some of the angles and of about 0.03 Å for some of the bonds cause significant changes in the vibrational spectra and, particularly, in the stretching modes. A detailed analysis of the SbF_6^- part in the previously reported²² spectra of $ClF_4^+SbF_6^-$ was not carried out due to complications caused by the presence of some $Sb_2F_{11}^-$ bands and an overlap with at least three fundamentals of ClF_4^+ , although the observed spectra²² appear to support the above conclusions.

Normal Coordinate Analyses. Normal coordinate analyses were carried out for the two isoelectronic series SF_4 , SeF_4 , TeF_4 and ClF_4^+ , BrF_4^+ , IF_4^+ . The results are summarized in Tables 16-21 and show that the A_2 , B_1 and B_2 vibrations are highly characteristic for all six compounds. For the A_1 block, however, strong mixing of the symmetry coordinates is observed. As previously discussed for ClF_4^+ ,²³ SF_4 ,^{23,53} and PF_4^- ,⁶¹ the ν_3 and ν_4 deformation modes are symmetric and antisymmetric combinations of the S_3 and S_4 symmetry coordinates, respectively. The ν_3 mode is the umbrella deformation, and ν_4 is the equatorial-axial ligand exchange motion involved in the Berry pseudorotation mechanism.⁵⁴ In addition to this mixing of the deformation modes, ν_1 which is mainly equatorial stretching, contains strong contributions from S_3 and S_4 that decrease with increasing mass of the central atom.

The force constants of greatest interest are the internal equatorial and axial stretching force constants (see Table 22 and Figure 5). The data exhibit the expected smooth trends and mass coupling effects, except for one surprising result. With increasing mass of the central atom, the equatorial stretching force constants decrease for the neutral XF_4 molecules while for the XF_4^+ cations they increase. This difference is due to the fact that the axial bonds in these pseudo-trigonal bipyramidal species contain different contributions from semi-ionic, 3center-4electron bonding.⁶³⁻⁶⁵ Semi-ionic bonding is favored by formal negative charges and, to a much lesser extent, by a decreasing mass of the central atom. Since the stretching force constants reflect only contributions from covalent bonding, their values for semi-ionic bonds should be only 50% of those of covalent bonds. As can be seen from Table 22, this is pretty much the case for PF_4^- ($f_R/f_r = 46\%$), while for SF_4 and ClF_4^+ this ratio increases to 65 and 87 %, respectively. These results show the importance of formal negative charges when comparing isoelectronic species containing semi-ionic bonds.

Another important point must be made concerning the force fields. In all the previously published force fields, the value of F_{44} , the axial, in plane bending force constant, had been badly underestimated by about 50% due to the undetermined nature of the previous A_1 block force constant solutions and the tempting low frequencies of ν_4 . The high values, found for F_{44} in this study, are in much better agreement with the well determined⁶² value of F_{99} , the axial out of plane bending force constant. Based on Gillespie's model of points an equal repulsion on a sphere,⁴³ the values of F_{44} and F_{99} should be of similar magnitude.

Conclusions

This paper provides the first comprehensive and conclusive study of the $\text{ClF}_5\cdot\text{SbF}_5$ adduct. It shows that $\text{ClF}_5\cdot\text{SbF}_5$ is ionic containing discrete ClF_4^+ and SbF_6^- ions that are interconnected and distorted by fluorine bridges. The ClF_4^+ cation has a pseudo-trigonal bipyramidal structure, in accord with the VSEPR predictions^{43,44} and the known structure of isoelectronic SF_4 .²⁴ The results of this study are supported by electronic structure calculations for the ClF_4^+ , BrF_4^+ , IF_4^+ and the isoelectronic SF_4 , SeF_4 , TeF_4 series. They permit a reassignment of the observed vibrational spectra and an analysis of their trends. Our results also show that the previously reported experimental structures and vibrational analyses of BrF_4^+ and IF_4^+ are inaccurate and/or incomplete and need to be repeated. Furthermore, it is shown that in these compounds fluorine bridging strongly distorts the individual ions. A simple method for modeling this bridging is described and can account for most of the differences between the experimental geometry and vibrational spectra of $\text{ClF}_4^+\text{SbF}_6^-$ and those predicted for the free isolated ions. It is also shown that the previous literature data for the closely related SF_4 , SeF_4 and TeF_4 molecules and BrF_4^+ and IF_4^+ ions need major revision.

Acknowledgements

The authors thank the National Science Foundation and the Air Force Office of Scientific Research for financial support.

Supporting Information Available

Tables of structure determination summary, atomic coordinates, bond lengths and angles and anisotropic displacement parameters of ClF_4SbF_6 in CIF format. This material is available free of charge via the internet at <http://pubs.acs.org>.

† Air Force Research Laboratory

‡ University of Southern California

References

1. Christe, K.O. *Proceedings from the XXIVth International Congress of Pure and Applied Chemistry* **1974**, 4, 115.
2. Christe, K.O.; Wilson, W.W.; Drake, G.W.; Dixon, D.A.; Boatz, J.A.; Gnann, R.Z. *J. Am. Chem. Soc.* **1998**, 120, 4711.
3. Christe, K.O.; Curtis, E.C.; Dixon, D.A. *J. Am. Chem. Soc.* **1993**, 115, 1520.
4. Musher, J.L. *Angew. Chem. Int. Ed. Engl.* **1968**, 8, 54.
5. Greenwood, N.N.; Earnshaw, A. *Chemistry of the Elements*, Pergamon Press, Oxford, 1986, p. 964-978.
6. Christe, K.O.; Sawodny, W. *Inorg. Chem.* **1969**, 8, 212.
7. Gillespie, R.J.; Morton, M.J. *Inorg. Chem.* **1970**, 9, 811.
8. Frenking, G.; Koch, W. *Inorg. Chem.* **1990**, 29, 4513.
9. Seel, F.; Detmer, O. *Angew. Chem.* **1958**, 70, 163; *Z. Anorg. Allgem. Chem.* **1959**, 301, 113.
10. Bartlett, N.; Lohmann, D.H. *J. Chem. Soc.* **1962**, 5253.
11. Selig, H.; Shamir, J. *Inorg. Chem.* **1964**, 3, 294.
12. Christe, K.O.; Pavlath, A.V. *Z. Anorg. Allgem. Chem.* **1965**, 335, 210.
13. Christe, K.O.; Sawodny, W. *Inorg. Chem.* **1967**, 6, 313.

14. Gillespie, R.J.; Morton, M.J. *Inorg. Chem.* **1970**, *9*, 616.
15. Edwards, A.J.; Sills, R.J.C. *J. Chem. Soc., A* **1970**, 2697.
16. Lynton, H.; Passmore, J. *Can. J. Chem.* **1971**, *49*, 2539.
17. Antipin, M. Yu.; Ellern, A.M.; Sukhoverkhov, V.F.; Struchkov, Yu. T.; Buslaev, Yu. A. *Russ. J. Inorg. Chem.* **1988**, *33*, 171.
18. Ellern, A.M.; Antipin, M. Yu.; Sharabarin, A.V.; Struchkov, Yu. T. *Russ. J. Inorg. Chem.* **1991**, *36*, 1278.
19. Bougon, R.; Cicha, W.V.; Lance, M.; Neublat, L.; Nierlich, M.; Vigner, J. *Inorg. Chem.* **1991**, *30*, 102.
20. Ellern, A.M.; Antipin, M. Yu.; Sharabarin, A.V.; Struchkov, Yu. T. *Russ. J. Inorg. Chem.* **1992**, *37*, 46.
21. Christe, K.O.; Pilipovich, D. *Inorg. Chem.* **1969**, *8*, 391.
22. Christe, K.O.; Sawodny, W. *Inorg. Chem.* **1973**, *12*, 2879.
23. Christe, K.O.; Curtis, E.C.; Schack, C.J.; Cyvin, S.J.; Brunvoll, J.; Sawodny, W. *Spectrochem. Acta, Part A* **1976**, *36*, 1141.
24. Tolles, W.M.; Gwinn, W.D. *J. Chem. Phys.* **1962**, *36*, 1119.
25. Lind, M.D.; Christe, K.O. *Inorg. Chem.* **1972**, *11*, 608.
26. Baird, H.W.; Giles, H.F. *Acta Cryst.* **1969**, *A25*, 115.
27. Edwards, A.J.; Taylor, P. *J. Chem. Soc. Dalton* **1975**, 2174.
28. Sawodny, W.; Birk, K.; Fogarasi, G.; Christe, K.O. *Z. Naturforsch* **1980**, *35B*, 1137, and references cited therein.
29. Sheldrick, G.M. Programs SHELX L86 and SHELX L93, University of Goettingen, Germany.

30. Frisch, M.J.; Trucks, G.W.; Schlegel, H.B.; Scuseria, G.E.; Robb, M.A.; Cheeseman, J.R.; Zakrzewski, V.G.; Montgomery, J.A., Jr.; Stratmann, R.E.; Burant, J.C.; Dapprich, S.; Millam, J.M.; Daniels, R.E.; Kudin, K.N.; Strain, M.C.; Farkas, O.; Tomasi, J.; Barone, V.; Cossi, M.; Cammi, R.; Mennucci, B.; Pomelli, C.; Adamo, C.; Clifford, S.; Ochterski, J.; Petersson, G.A.; Ayala, P.Y.; Cui, Q.; Morokuma, K.; Malick, D.K.; Rabuck, A.D.; Raghavachari, K.; Foresman, J.B.; Cioslowski, J.; Ortiz, J.V.; Stefanov, B.B.; Liu, G.; Liashenko, A.; Piskorz, P.; Komaromi, I.; Gomperts, R.; Martin, R. L.; Fox, D. J.; Keith, T.; Al-Laham, M. A.; Peng, C.Y.; Nanayakkara, A.; Gonzalez, C.; Challacombe, M.; Gill, P.M.W.; Johnson, B.; Chen, W.; Wong, M.W.; Andres, J.L.; Gonzalez, C.; Head-Gordon, M.; Replogle, E.S.; Pople, J.A. *Gaussian 98*, revision A.6; Gaussian, Inc.: Pittsburgh, PA, 1998.
31. Stanton, J.F.; Gauss, J.; Watts, J.D.; Nooijen, M.; Oliphant, N.; Perera, S.A.; Szalay, P.G.; Lauderdale, W.J.; Gwaltney, S.R.; Beck, S.; Balkova, A.; Bernholdt, D.E.; Baeck, K.K.; Rozyczko, P.; Sekino, H.; Hober, C.; Bartlett, R.J. *ACES II, Quantum Theory Project*; University of Florida: Integral packages included are VMOL (Almlöf, J.; Taylor, P.R.), BPROPS (Taylor, P.R.), and ABACUS (Helgaker, T.; Jensen, H.J.Aa.; Jorgensen, P.; Olsen, J.; Taylor, P.R.)
32. The B3LYP functional uses a three-parameter exchange functional of Becke (B3) [Becke, A.D. *J. Chem. Phys.* **1993**, 98, 5648; Stephens, P.J.; Devlin, C.F.; Chabalowski, C.F.; Frisch, M.J. *J. Phys. Chem.* **1994**, 98, 11623] and the Lee, Yang, and Parr (LYP) correlation gradient-corrected functional [Lee, C.; Yang, W.; Parr, R.G. *Phys. Rev. B* **1988**, 37, 785].
33. a) Pople, J.A.; Binkley, J.S.; Seeger, R. *Int. Quantum Chem.* **1976**, 10, 1.

- b) Bartlett, R.J.; Silver, D.M. *Int. Quantum Chem.* **1975**, 9, 183.
- c) Dupuis, M.; Chin, S.; Marquez, A. in G. Malli (ed.), *Relativistic and Electron Correlation Effects in Molecules*, Plenum, New York, 1994.
- d) Frisch, M.J.; Head-Gordon, M.; Pople, J.A. *Chem. Phys. Lett.* **1990**, 166, 275.
- e) Bartlett, R.J.; Stanton, R.J. Applications of post-Hartree-Fock methods: A Tutorial, in: Lipkowitz, K.B.; Boyd, D.B. (Eds.), *Reviews of Computational Chemistry*, Vol. V, VCH Publishers, New York, 1994.
34. Purvis, G.D., III; Bartlett, R.J. *J. Chem. Phys.* **1982**, 76, 1910.
35. Raghavachari, K.; Trucks, G.W.; Pople, J.A.; Head-Gordon, M. *Chem. Phys. Lett.* **1989**, 157, 479.
36. These local-spin-density-optimized Gaussian basis sets were developed by Nathalie Godbout and Jan Andzelm, and are made available courtesy of Cray Research, Inc. The general method by which they were developed is given in: Godbout, N.; Salahub, D.R.; Andzelm, J.; Wimmer, E. *Can. J. Chem.* **1992**, 70, 560.
37. Basis sets were obtained from the Extensible Computational Chemistry Environment Basis Set Database, Version , as developed and distributed by the Molecular Science Computing Facility, Environmental and Molecular Sciences Laboratory which is part of the Pacific Northwest Laboratory, P.O. Box 999, Richland, Washington 99352, USA, and funded by the U.S. Department of Energy. The Pacific Northwest Laboratory is a multi-program laboratory operated by Battelle Memorial Institute for the U.S. Department of Energy under contract DE-AC06-76RLO 1830. Contact David Feller or Karen Schuchardt for further information.
38. a) Woon, D. E.; Dunning, Jr., T. H. *J. Chem. Phys.* **1993**, 98, 1358.

- b) Wilson, A. K.; Woon, D. E.; Peterson, K. A.; Dunning, Jr., T. H. *J. Chem. Phys.* **1999**, *110*, 7667.
39. Polarization functions are unpublished supplements to the basis sets described in: Schafer, A.; Huber, C.; Ahlrichs, R. *J. Chem. Phys.* **1994**, *100*, 5829.
40. Frisch, M. J.; Pople, J. A.; Binkley, J. S. *J. Chem. Phys.* **1984**, *80*, 3265.
41. Schmidt, M.W.; Baldridge, K.K.; Boatz, J.A.; Elbert, S.T.; Gordon, M.S.; Jensen, J.H.; Koseki, S.; Matsunaga, N.; Nguyen, K.A.; Su, S.J.; Windus, T.L.; Dupuis, M.; Montgomery, J.A. *J. Comput. Chem.* **1993**, *14*, 1347.
42. Komornicki, A. *Bmtrx*, Version 2.0; Polyatomics Research Institute: Redwood City, CA 1996.
43. Bondi, A. *J. Phys. Chem.* **1964**, *68*, 441.
44. Gillespie, R.J.; Hargittai, I. *The VSEPR Model of Molecular Geometry*, Allyn and Bacon, Boston, **1991**, p.55.
45. Gillespie, R.J.; Robinson, E.A. *Angew. Chem. Int. Ed. Engl.* **1996**, *35*, 495.
46. Bowater, I.C.; Brown, R.D.; Burden, F.R. *J. Mol. Spectrosc.* **1968**, *28*, 454.
47. Ungemach, S.R.; Schaefer, H.F., III. *J. Am. Chem. Soc.* **1976**, *98*, 1658; *Chem. Phys. Lett.* **1976**, *38*, 407.
48. So, S-P. *J. Chem. Soc., Faraday Trans. II* **1981**, *77*, 213.
49. Pershin, V.L.; Boldyrev, A.I. *J. Mol. Struct. (Theochem.)* **1987**, *150*, 171.
50. Minyaev, R.M. *Russ. J. Inorg. Chem.* **1993**, *38*, 1300.
51. Minyaev, R.M.; Wales, D.J. *J. Chem. Soc., Faraday Trans.* **1994**, *90*, 1831.
52. Schleyer, P.v.R.; Mauksch, M. private communication.
53. Christie, K.O.; Sawodny, W.; Pulay, P. *J. Mol. Structure* **1974**, *21*, 158.
54. Berry, R.S. *J. Chem. Phys.* **1960**, *32*, 933.
55. Adams, C.J.; Downs, A.J. *Spectrochim. Acta* **1972**, *28A*, 1841.

56. Alexander, L.E.; Beattie, I.R. *J. Chem. Soc. Dalton* **1972**, 1745.
57. Ramaswamy, K.; Jayaraman, S. *Ind. J. Pure Appl. Phys.* **1970**, 8, 625.
58. Seppelt, K. *Z. Anorg. Allg. Chem.* **1975**, 416, 12.
59. Nakamoto, K. "Infrared and Raman Spectra of Inorganic and Coordination Compounds," John Wiley & Sons, New York, Fifth Edition, 1997.
60. Edwards, A.J.; Hewaidy, F.I. *J. Chem. Soc. A* **1968**, 3977.
61. Christe, K.O.; Dixon, D.A.; Mercier, H.P.A.; Sanders, J.P.C.; Schrobilgen, G.J.; Wilson, W.W. *J. Am. Chem. Soc.* **1994**, 116, 2850.
62. Christe, K.O.; Willner, H.; Sawodny, W. *Spectrochim. Acta* **1979**, 35A, 1347.
63. Pimentel, G.C. *J. Chem. Phys.* **1951**, 19, 446.
64. Hach, R.J.; Rundle, R.E. *J. Am. Chem. Soc.* **1951**, 73, 4321.
65. Rundle, R.E. *J. Am. Chem. Soc.* **1963**, 85, 112.

Table 1. Crystal data for $[\text{ClF}_4]^+[\text{SbF}_6]^-$

Empirical formula	Cl F ₁₀ Sb
Formula weight	347.20
Temperature	193(2) K
Wavelength	0.71073 Å
Crystal system	Orthorhombic
Space Group	Pbcm (#57)
Unit cell dimensions	a = 5.9546(12) Å alpha = 90 deg. b = 15.1717(19) Å beta = 90 deg. c = 7.9598(17) Å gamma = 90 deg.
Volume	719.7(2) Å ³
Z	4
Final R indices [I > 2 sigma(I)]	R1 = 0.0220, wR2 = 0.0493 (854 data)
R indices (all data)	R1 = 0.0227, wR2 = 0.0496 (880 data)

Table 2. Atomic coordinates ($\times 10^4$) and equivalent isotropic displacement parameters ($\text{\AA}^2 \times 10^3$) for $[\text{ClF}_4]^+[\text{SbF}_6]^-$. $U(\text{eq})$ is defined as one third of the trace of the orthogonalized U_{ij} tensor.

	x	y	z	$U(\text{eq})$
Sb	904(1)	1402(1)	2500	15(1)
F(1)	-1565(4)	2191(1)	2500	25(1)
F(2)	-1047(4)	445(2)	2500	37(1)
F(3)	2845(4)	2392(1)	2500	26(1)
F(4)	902(3)	1429(1)	162(3)	34(1)
F(5)	3413(4)	669(1)	2500	33(1)
Cl	5883(1)	3440(1)	2500	16(1)
F(11)	4042(3)	4140(1)	2500	24(1)
F(12)	8045(4)	3987(1)	2500	25(1)
F(13)	5900(3)	3496(1)	472(2)	33(1)

Table 3. Bond lengths [\AA] and angles [$^\circ$] for $[\text{ClF}_4]^+[\text{SbF}_6]^-$.

Sb-F(2)	1.860(2)
Sb-F(4)	1.863(2)
Sb-F(5)	1.863(2)
Sb-F(3)	1.895(2)
Sb-F(1)	1.896(2)
Cl-F(11)	1.527(2)
Cl-F(12)	1.532(2)
Cl-F(13)	1.617(2)
Cl...F(1*)	2.43
Cl...F(3*)	2.41
F(2)-Sb-F(4)	90.97(5)
F(4)-Sb-F(4*)	177.47(9)
F(2)-Sb-F(5)	91.99(10)
F(4)-Sb-F(5)	90.78(5)
F(2)-Sb-F(3)	178.95(9)
F(4)-Sb-F(3)	89.02(5)
F(5)-Sb-F(3)	89.06(9)
F(2)-Sb-F(1)	90.49(11)
F(4)-Sb-F(1)	89.18(5)
F(5)-Sb-F(1)	177.53(9)
F(3)-Sb-F(1)	88.47(9)
F(11)-Cl-F(12)	103.08(12)
F(11)-Cl-F(13)	88.16(6)
F(12)-Cl-F(13)	88.06(6)
F(13)-Cl-F(13*)	173.92(13)
F(11)-Cl...F(3*)	85.4
F(12)-Cl...F(1*)	84.0
F(1*)...Cl...F(3*)	87.5

Table 4. Observed and calculated geometries^a of SF₄

	obsd ^b	calcd ^c		
		B3LYP	MP2	CCSD(T)
r (S-F _{eq})	1.545(3)	1.579	1.563	1.563
r (S-F _{ax})	1.646(3)	1.681	1.660	1.657
< (F _{eq} -S-F _{eq})	101.5(5)	101.3	101.6	101.4
< (F _{ax} -S-F _{ax})	173.1(5)	172.4	171.9	171.6

^aBond distances in Å, angles in degrees. ^bData from ref 24.

^cThe following basis set was used for all calculations: S: DFT-DZVP; F: 6-311 + G(2d).

Table 5. Observed and calculated geometries^a of SeF₄ and TeF₄

	SeF ₄				TeF ₄ ^c		
	obsd ^b	calcd ^d			calcd ^d		
		B3LYP	MP2	CCSD(T)	B3LYP	MP2	CCSD(T)
r (X-F _{eq})	1.682(4)	1.718	1.701	1.703	1.879	1.862	1.866
r (X-F _{ax})	1.771(4)	1.805	1.784	1.784	1.939	1.924	1.926
< (F _{eq} -X-F _{eq})	100.6(7)	100.6	101.0	100.9	103.1	101.0	101.1
< (F _{ax} -X-F _{ax})	169.2(7)	169.2	168.1	167.5	159.4	161.2	160.5

^aBond distances in Å, angles in degrees. ^bData from ref 46. ^cTeF₄ is polymeric under normal conditions (ref 60) and no experimental structure for free TeF₄ is presently known. ^dThe following basis sets were used for all calculations: Se: DFT-DZVP + f(0.462); Te:DFT-DZVP + f(0.474); F: 6-311 + G(2d).

Table 6. Observed and calculated geometries^a of ClF_4^+

	obsd ^b $\text{ClF}_4^+\text{SbF}_6^-$	calcd ^b , free ClF_4^+			predicted free ClF_4^+
		B3LYP	MP2	CCSD(T)	
$r(\text{Cl-F}_{\text{eq}})$	1.530(2)	1.577	1.543	1.557	1.539
$r(\text{Cl-F}_{\text{ax}})$	1.618(2)	1.635	1.612	1.615	1.604
$\angle(\text{F}_{\text{eq}}\text{-Cl-F}_{\text{eq}})$	103.08(12)	107.8	107.1	107.7	107.7
$\angle(\text{F}_{\text{ax}}\text{-Cl-F}_{\text{ax}})$	173.92(13)	172.2	172.3	171.4	173.0

^aBond distances in Å, angles in degrees. ^bThe following basis set was used for all calculations:

Cl:DFT-DZVP + f(0.706) from cc-pVTZ; F: 6-311+ G(2d).

Table 7. Observed and calculated geometries^a for BrF₄⁺ and IF₄⁺

	BrF ₄ ⁺				IF ₄ ⁺			
	obsd ^b	calcd ^d			obsd ^c	calcd ^d		
	BrF ₄ ⁺ Sb ₂ F ₁₁ ⁻	B3LYP	MP2	CCSD(T)	IF ₄ ⁺ Sb ₂ F ₁₁ ⁻	B3LYP	MP2	CCSD(T)
r (X-F _{eq})	1.77(12)	1.700	1.672	1.683	1.77(3)	1.838	1.818	1.823
r (X-F _{ax})	1.86(12)	1.749	1.728	1.732	1.85(4)	1.875	1.861	1.863
< (F _{eq} -X-F _{eq})	95.5(50)	104.9	104.9	105.4	92.4(12)	106.8	103.8	104.2
< (F _{ax} -X-F _{ax})	173.5(61)	168.8	168.2	167.2	160.3(12)	158.3	161.2	160.3

^aBond distances in Å, angles in degrees. ^bData from ref 25. ^cAveraged bond lengths from ref 27.

^dThe following basis sets were used for all calculations: Br: DFT-DZVP + f(0.552) from cc-pVTZ; I: DFT-DZVP + f(0.486); F: -311 + G(2d).

Table 8. Geometries^a of $\text{ClF}_4^+ \cdot 2\text{HF}$ and free ClF_4^+ compared to that of ClF_4^+ in $\text{ClF}_4^+\text{SbF}_6^-$

	calculated ^b , B3LYP		observed ^c
	free ClF_4^+	$\text{ClF}_4^+ \cdot 2\text{HF}$	$\text{ClF}_4^+\text{SbF}_6^-$
$r(\text{Cl-F}_{\text{eq}})$	1.577	1.582	1.530(2)
$r(\text{Cl-F}_{\text{ax}})$	1.635	1.653	1.618(2)
$\angle(\text{F}_{\text{eq}}\text{-Cl-F}_{\text{eq}})$	107.8	100.8	103.08(12)
$\angle(\text{F}_{\text{ax}}\text{-Cl-F}_{\text{ax}})$	172.2	172.8	173.92(13)

^aBond distances in Å, angles in degrees. ^bThe same basis set as in Table 6 was used. ^cData from this study.

Table 9. Observed and scaled (unscaled) calculated vibrational frequencies of SF₄

species approx mode description			frequencies, cm ⁻¹			
			obsd ^b	calcd ^c		
				B3LYP	MP2	CCSD(T)
A ₁	ν_1	vsym SF ₂ eq	892	889 (856) [117, 14p] ^d	887 (904) [125, 12p]	881 (900) [120]
	ν_2	vsym SF ₂ ax	558	557 (537) [3.1, 12p]	558 (569) [3.2, 12p]	561 (573) [3.4]
	ν_3	sym comb of δ sciss SF ₂ eq and ax	532	537 (494) [22, 2.1p]	539 (531) [26, 1.7p]	538 (533) [26]
	ν_4	asym comb of δ sciss SF ₂ eq and ax	228	226 (208) [1.2, .51p]	226 (223) [1.0, 40p]	226 (224) [.89]
A ₂	ν_5	τ SF ₂	475	473 (435) [0, 1.2dp]	471 (464) [0, 1.0dp]	470 (465) [0]
B ₁	ν_6	vas SF ₂ ax	730	741 (714) [659, 1.1dp]	739 (753) [693, 1.2dp]	740 (756) [680]
	ν_7	δ rock SF ₂ eq	[~532] ^e	540 (497) [.21, .54dp]	539 (531) [.43, .53dp]	538 (533) [.85]
B ₂	ν_8	vas SF ₂ eq	867	858 (827) [187, 5.0dp]	862 (879) [196, 4.3dp]	862 (881) [184]
	ν_9	δ sciss SF ₂ ax out of plane	353	354 (326) [12, 0.1dp]	353 (348) [13, .06dp]	356 (352) [14]
sum of (ν obsd \pm ν calcd)				34	32	45
empirical scal. factors: ν				1.03798	0.98080	.97866
δ				1.08696	1.01559	1.01008

^aSeparate empirical scaling factors were used for the stretching and deformation vibrations to maximize the fit between observed and calculated frequencies. ^bData from ref 28. ^cUsing basis set from Table 4. ^dCalculated infrared and Raman intensities in km/mol and Å⁴/AMU. ^eThis band coincides with and is obscured by ν_3 .

Table 10. Observed and scaled (unscaled) calculated^a vibrational frequencies of ClF_4^+

vibration		frequencies, cm^{-1}			
		obsd for $\text{ClF}_4^+\text{SbF}_6^-$	calcd for free ClF_4^+		
			B3LYP	MP2	CCSD(T)
A_1	ν_1	802[vs, 10] ^b	778 (769) [49, 19p] ^c	803 (856) [64, 11p]	774 (794) [49]
	ν_2	574 [w, 6]	583 (576) [6.0, 18p]	568 (605) [5.7, 13p]	583 (598) [4.7]
	ν_3	515 [sh, 0.2]	506 (475) [21, 3.1p]	515 (526) [26, 1.7p]	508 (509) [24]
	ν_4	235 [-, 0.5]	150 (141) [.55, 1.1wp]	166 (169) [.69, .76wp]	159 (159) [.50]
A_2	ν_5	475 [-, 1]	488 (458) [0, 2.4dp]	488 (498) [0, 2.0dp]	488 (489) [0]
B_1	ν_6	803 [vs, ?]	841 (831) [437, .11dp]	809 (862) [478, .23dp]	833 (855) [428]
	ν_7	534 [mw, 1]	538 (505) [5.5, 1.2dp]	541 (552) [7.3, 1.0dp]	537 (538) [8.7]
B_2	ν_8	822 [s, 2.5]	798 (788) [116, 5.0dp]	824 (878) [146, 2.9dp]	810 (831) [102]
	ν_9	386 [m, -]	379 (356) [15, .23dp]	371 (379) [18, .14dp]	379 (380) [18]
sum of (ν obsd \pm ν calcd)			213	119	185
empirical scal. factors ^d : ν			1.01222	.93836	0.97457
δ			1.06576	.97969	0.99788


^aUsing basis set from Table 6. ^bObserved relative infrared and Raman intensities. ^cCalculated infrared and Raman intensities in km/mol and $\text{\AA}^4/\text{AMU}$. ^d ν_4 was omitted from the calculation of the scaling factors for the deformation modes.

Table 11. Scaled (unscaled) vibrational frequencies of free gaseous ClF_4^+ and $\text{ClF}_4^+ \cdot 2\text{HF}$, calculated at the B3LYP level, compared to those observed for $\text{ClF}_4^+\text{SbF}_6^-$

mode	approx mode description	obsd in $\text{ClF}_4^+\text{SbF}_6^-$	calculated	
			free ClF_4^+	$\text{ClF}_4^+ \cdot 2\text{HF}^b$
A ₁	ν_1 vsym ClF_2eq	802	778 (769)	794 (766) [147,50p]
	ν_2 vsym ClF_2ax	574	583 (576)	577 (557) [7.9, 20p]
	ν_3 $\delta\text{sciss ClF}_2\text{eq}$ and ax, sym combination	515	506 (475)	517 (476) [60, 2.3p]
	ν_4 $\delta\text{sciss ClF}_2$ eq and ax, antisym combination	235	150 (141)	225 (206) ^c [.96, .92p]
A ₂	ν_5 τClF_2	475	488 (458)	470 (439) [0, 1.9dp]
B ₁	ν_6 vas ClF_2ax	803	841 (831)	831 (802) [481, .47dp]
	ν_7 $\delta\text{rock ClF}_2\text{eq}$	534	538 (505)	538 (496) [1.9, .89dp]
B ₂	ν_8 vas ClF_2eq	822	798 (788)	798 (770) [167, 15dp]
	ν_9 $\delta\text{sciss ClF}_2\text{ax}$ out of plane	386	379 (356)	399 (367) [39, .08dp]
$\Sigma\Delta$ (ν obsd \pm ν calcd)			213	92
scaling factors: ν			1.01222	1.036575
δ			1.06576	1.08544

^aEmpirical scaling factors to maximize the fit. ^bThe two Cl-F contacts between ClF_4^+ and 2HF were constrained to 2.42 Å, the observed Cl-F bridge distance in $\text{ClF}_4^+\text{SbF}_6^-$. ^cThis mode couples with the symmetric ClF_2 bridge stretching mode as a symmetric and an antisymmetric combination of the corresponding symmetry coordinates. The listed frequency of 206 cm^{-1} is the average of the calculated values of 185 and 227 cm^{-1} (see Table 12).

Table 12. Calculated unscaled fluorine bridge modes in $\text{ClF}_4^+ \cdot 2\text{HF}^a$

		approximate mode description in symmetry C_{2v}	B3LYP freq [IR, Ra int]
A ₁	v ₁ '	antisymmetric and symmetric combinations of the symmetric $\text{ClF}_{2\text{BR}}$ stretch and the ClF_4^+ Berry mode v ₄	{ 227 [0.96, .92p] 185 [1.0, 2.5p]
	v ₂ '	δsciss $\text{ClF}_{2\text{BR}}$	62 [3.2, .48p]
A ₂	v ₃ '	δpucker	55 [0, 1.2dp]
			
B ₁	v ₄ '	δrock $\text{ClF}_{2\text{BR}}$	71 [49, 1.6dp]
B ₂	v ₅ '	vas $\text{ClF}_{2\text{BR}}$	178 [11, .97dp]
	v ₆ '	δas $\text{ClF}_{2\text{BR}}$ in plane	132 [0.2, .02dp]

^aIn addition to these 6 modes, the following 6 modes were identified which involve hydrogen displacements: 3951, νH-F, in phase; 3947, νH-F, out of phase; 308, δwag H, in phase; 301, δwag H, out of phase; -83, δrock H, out of phase; -38, δrock H, in phase.

Table 13. Observed and scaled^a (unscaled) calculated vibrational frequencies (cm⁻¹) of SeF₄ and TeF₄

Vibration ^b		SeF ₄			TeF ₄		
		calcd			calcd		
Obsd					obsd		
		B3LYP	MP2	CCSD(T)	B3LYP	MP2	CCSD(T)
A ₁	v ₁	744	743(723)[60,16p] ^c	736(754)[59]	695	680(674)[56,16p]	680(102)[57]
	v ₂	574	581(565)[1.7,14p]	580(595)[.75]	572	572(567)[.02,12p]	570(589)[0.07]
	v ₃	367	369(339)[25,1.2p]	372(369)[31]	293	294(271)[33,.96p]	297(291)[40]
	v ₄	162	169(155)[1.6,.58wp]	167(165)[1.4]	—	107(99)[1.1,.38wp]	125(122)[0.9]
A ₂	v ₅	374	372(342)[0,1.6dp]	372(367)[0]	—	323(298)[0,1.3dp]	312(305)[0]
B ₁	v ₆	634	635(618)[378,.73dp]	637(653)[381]	588	606(600)[257,1.8dp]	607(627)[268]
	v ₇	409	407(374)[10,1.0dp]	400(405)[16]	333	332(306)[15,.84dp]	328(321)[20]
B ₂	v ₈	733	724(705)[117,5.6dp]	730(748)[114]	682	676(670)[104,5.9dp]	678(700)[101]
	v ₉	256	248(228)[14,.02dp]	249(246)[15]	—	222(205)[14,0]	199(195)[15]
ΣΔ(V obsd ± V calcd)		39	36	43	41	48	49
Empirical scaling V		1.02765	0.97188	0.97557	1.00947	0.9668	0.96831
Factors δ		1.08754	1.01176	1.01176	1.08471	1.02055	1.02213

Table 14. Observed and scaled^a (unscaled) calculated vibrational frequencies (cm⁻¹) of BrF₄⁺ and IF₄⁺

Vibration ^b		BrF ₄ ⁺		IF ₄ ⁺	
		Obsd	calcd	calcd	
		B3LYP	MP2	CCSD(T)	
A ₁	ν ₁	723	718(721)[23,21p]	729(783)[31,13p]	708(738)[21]
	ν ₂	606	622(625)[2,18p]	612(658)[1.5,14p]	623(650)[.94]
	ν ₃	369	366(351)[21,1.5p]	368(385)[25,1.1p]	368(377)[25]
	ν ₄		137(131)[.71,.97wp]	141(147)[.7,8p]	139(143)[.62]
A ₂	ν ₅	385	388(372)[0,2.5dp]	386(403)[0,2.3dp]	386(396)[0]
	ν ₆	736	730(733)[253,.16dp]	716(769)[272,.3dp]	731(762)[242]
B ₁	ν ₇		414(397)[12,1.4dp]	411(430)[16,1.3dp]	410(420)[16]
	ν ₈	736	729(732)[68,5.6dp]	743(798)[86,3.4dp]	737(768)[59]
B ₂	ν ₉		272(261)[13,.06dp]	262(274)[14,.04dp]	269(276)[14]
ΣΔ(V obsd ± V calcd)			40	41	40
Empirical scaling V			.99548	0.93128	0.95905
Factors δ			1.04311	0.95689	0.97550

^aEmpirical scaling factors. ^bThe approximate mode description is identical to that given in Table 9.

Table 15. Correlation diagram for SbF_6^- ($O_h \rightarrow C_{2v}$) and unscaled frequencies, infrared and Raman intensities, and polarization of Raman bands calculated at the B3LYP level

O_h		C_{2v}	
609[0,24p] A_{1g}	_____	A_1	612 [18, 19p]
552[0,2.9dp] E_g	_____	A_1	557 [3.3, 5.0p]
	_____	B_2	538 [3.4, 2.9 dp]
647[647,0] F_{1u}	_____	A_1	635 [163, 2.7p]
	_____	B_1	674 [182, .0001 dp]
	_____	B_2	633[181, .04dp]
294[63, 0] F_{1u}	_____	A_1	286 [64, .0014p]
	_____	B_1	287 [63, .0015 dp]
	_____	B_2	286[64, 0]
268[0,1.5dp] F_{2g}	_____	A_1	256 [.04, 1.5dp]
	_____	A_2	264 [0, 1.5 dp]
	_____	B_1	264[.05, 1.5dp]
174[0, 0] F_{2u}	_____	A_1	166 [.09, 0]
	_____	A_2	171 [0, 0]
	_____	B_2	166[.09, 0]

Table 16. Scaled CCSD(T) force constants and potential energy distribution of SF₄

				symmetry force constants ^b				potential energy ^c distribution (%)
				F ₁₁	F ₂₂	F ₃₃	F ₄₄	
A ₁	v ₁	881	F ₁₁	5.40				60(1), 4(2), 15(3), 21(4)
	v ₂	561	F ₂₂	.78	3.81			90(2), 10(1)
	v ₃	538	F ₃₃	.19	-.01	1.22		55(4), 41(3), 3(1)
	v ₄	226	F ₄₄	.45	-.10	.60	1.49	59(3), 41(4)
A ₂	v ₅	470	F ₅₅	1.97				100(5)
B ₁	v ₆	740	F ₆₆	F ₆₆	F ₇₇			
				2.99				74(6), 26(7)
	v ₇	538	F ₇₇	0.74	2.19			96(7), 4(6)
B ₂	v ₈	862	F ₈₈	F ₈₈	F ₉₉			
				5.01				89(8), 11(9)
	v ₉	356	F ₉₉	.56	1.98			100(9)

^aFrequencies from Table 9. ^bStretching force constants in mdyn/Å, deformation constants in mdyn Å/rad², and stretch-bend interaction constants in mdyn/rad. Scaling factors: stretching force constants, (.97866)²; deformation constants, (1.01008)²; stretch-bend interactions, .97866 x 1.01008. ^cThe following symmetry coordinates were used:

S1 = vsym eq; S2 = vsym ax; S3 = δsym eg; S4 = δsym ax; S5 = τ; S6 = vas ax; S7 = δ rock eq; S8 = vas eq; S9 = δsciss ax out of plane.

Table 17. Scaled CCSD(T) force constants and potential energy distribution of SeF₄

calcd freq, ^a cm ⁻¹				symmetry force constants ^b				potential energy ^c distribution (%)
				F ₁₁	F ₂₂	F ₃₃	F ₄₄	
A ₁	v ₁	736	F ₁₁	4.89				84(1), 7(2), 4(3), 5(4)
	v ₂	580	F ₂₂	0.39	3.89			91(2), 9(1)
	v ₃	372	F ₃₃	.02	-.02	.95		52(4), 47(3), 1(2)
	v ₄	167	F ₄₄	.22	-.22	.49	1.01	52(3), 48(4)
A ₂	v ₅	372	F ₅₅	1.46				100(5)
B ₁	v ₆	637	F ₆₆	F ₆₆	F ₇₇			
				3.17				94(6), 6(7)
	v ₇	400	F ₇₇	0.36	1.63			100(7), 4(6)
B ₂	v ₈	730	F ₈₈	F ₈₈	F ₉₉			
				4.69				98(8), 2(9)
	v ₉	249	F ₉₉	.25	1.39			100(9)

^aFrequencies from Table 13. ^{b,c}Force constant dimensions and symmetry coordinates are identical to those given in the footnotes of Table 16. Scaling factors – stretching force constants, (.97557)²; deformation constants, (1.01281)²; stretch-bend interaction, .97557 x 1.01281.

Table 18. Scaled CCSD(T) force constants and potential energy distribution of TeF₄

				calcd freq, ^a cm ⁻¹				symmetry force constants ^b				potential energy ^c distribution (%)
								F ₁₁	F ₂₂	F ₃₃	F ₄₄	
A ₁	v ₁	680	F ₁₁	4.52								90(1), 7(2), 2(3), 2(4)
	v ₂	570	F ₂₂	0.23	3.69							93(2), 7(1)
	v ₃	297	F ₃₃	-.076	-.039	.76						53(4), 47(3)
	v ₄	125	F ₄₄	.17	-.19	.48	.84					52(3), 46(4)
A ₂	v ₅	312	F ₅₅	1.22								100(5)
				F ₆₆	F ₇₇							
B ₁	v ₆	607	F ₆₆	3.25								98(6), 2(7)
	v ₇	328	F ₇₇	0.20	1.37							100(7)
				F ₈₈	F ₉₉							
B ₂	v ₈	678	F ₈₈	4.40								99(8), 1(9)
	v ₉	199	F ₉₉	.15	1.12							100(9)

^aFrequencies from Table 13. ^{b,c}Force constant dimensions and symmetry coordinates are identical to those given in the footnotes of Table 16. Scaling factors – stretching force constants, (.96831)²; deformation constants, (1.02213)²; stretch-bend interaction, .96831 x 1.02213.

Table 19. Scaled CCSD(T) force constants and potential energy distribution of ClF_4^+

				symmetry force constants ^b				potential energy ^c distribution (%)
calcd freq, ^a cm ⁻¹				F ₁₁	F ₂₂	F ₃₃	F ₄₄	
A ₁	v ₁	774	F ₁₁	4.46				58(1), 5(2), 16(3), 21(4)
	v ₂	583	F ₂₂	.47	3.97			87(2), 11(1), 1(3), 1(4)
	v ₃	508	F ₃₃	.020	-0.027	.73		62(4), 34(3), 4(1)
	v ₄	159	F ₄₄	.46	-.018	.60	1.35	69(3), 30(4)
A ₂	v ₅	488	F ₅₅	2.01				100(5)
				F ₆₆	F ₇₇			
B ₁	v ₆	833	F ₆₆	3.89				77(6), 23(7)
	v ₇	537	F ₇₇	0.69	2.21			98(7), 2(6)
				F ₈₈	F ₉₉			
B ₂	v ₈	810	F ₈₈	4.53				89(8), 11(9)
	v ₉	379	F ₉₉	.69	2.03			100(9)

^aFrequencies from Table 10. ^{b,c}Force constant dimensions and symmetry coordinates are identical to those given in the footnotes of Table 16. Scaling factors – stretching force constants, (.97457)²; deformation constants, (.99788)²; stretch-bend interaction, .97457 x 0.99788.

Table 20. Scaled CCSD(T) force constants and potential energy distribution of BrF_4^+

				symmetry force constants ^b				potential energy ^c distribution (%)
				F ₁₁	F ₂₂	F ₃₃	F ₄₄	
A ₁	v ₁	708	F ₁₁	4.68				84(1), 7(2), 4(3), 5(4)
	v ₂	623	F ₂₂	.15	4.40			91(2), 9(1)
	v ₃	368	F ₃₃	-.009	.012	.70		60(4), 40(3)
	v ₄	139	F ₄₄	.27	-.11	.49	.98	62(3), 38(4)
A ₂	v ₅	386	F ₅₅	1.48				100(5)
				F ₆₆	F ₇₇			
B ₁	v ₆	731	F ₆₆	4.12				93(6), 7(7)
	v ₇	410	F ₇₇	.35	1.65			100(7)
				F ₈₈	F ₉₉			
B ₂	v ₈	737	F ₈₈	4.74				97(8), 3(9)
	v ₉	269	F ₉₉	.36	1.44			100(8)

^aFrequencies from Table 14. ^{b,c}Force constant dimensions and symmetry coordinates are identical to those given in the footnotes of Table 16. Scaling factors – stretching force constants, (.95905)²; deformation constants, (.97550)²; stretch-bend interaction, .95905 x .97550.

Table 21. Scaled CCSD(T) force constants and potential energy distribution of IF_4^+

				symmetry force constants ^b				potential energy ^c distribution (%)
calcd freq, ^a cm ⁻¹				F ₁₁	F ₂₂	F ₃₃	F ₄₄	
A ₁	v ₁	710	F ₁₁	5.01				92(1), 5(2), 1(3), 2(4)
	v ₂	640	F ₂₂	.056	4.59			95(2), 5(1)
	v ₃	307	F ₃₃	.011	.046	.73		57(4), 43(3)
	v ₄	131	F ₄₄	.23	-.088	.46	.87	43(4), 57(3)
A ₂	v ₅	329	F ₅₅	1.30				100(5)
				F ₆₆	F ₇₇			
B ₁	v ₆	703	F ₆₆	4.32				98(6), 2(7)
	v ₇	345	F ₇₇	.23	1.37			100(7)
				F ₈₈	F ₉₉			
B ₂	v ₈	728	F ₈₈	5.07				99(8), 1(9)
	v ₉	211	F ₉₉	.24	1.19			100(9)

^aEmpirical scaling factors of .96 and .98 were used for the stretching and deformation modes respectively.. ^{b,c}Force constant dimensions and symmetry coordinates are identical to those given in the footnotes of Table 16. Scaling factors – stretching force constants, (.96)²; deformation constants, (.98)²; stretch-bend interaction, .96 x .98.

Table 22. Stretching force constants (mdyn / Å) of ClF_4^+ and SF_4 compared to those of PF_4^- , SeF_4 , TeF_4 , BrF_4^+ and IF_4^+

	PF_4^-	SF_4	SeF_4	TeF_4	ClF_4^+	BrF_4^+	IF_4^+
fr, eq	3.94	5.21	4.79	4.46	4.50	4.77	5.04
frr	.26	.20	.10	.06	-.035	-.03	-.03
fR, ax	1.82	3.40	3.53	3.47	3.93	4.26	4.46
fRR	.34	.41	.36	.22	.04	.14	.14
fR/fr	.46	.65	.74	.78	.87	.89	.88

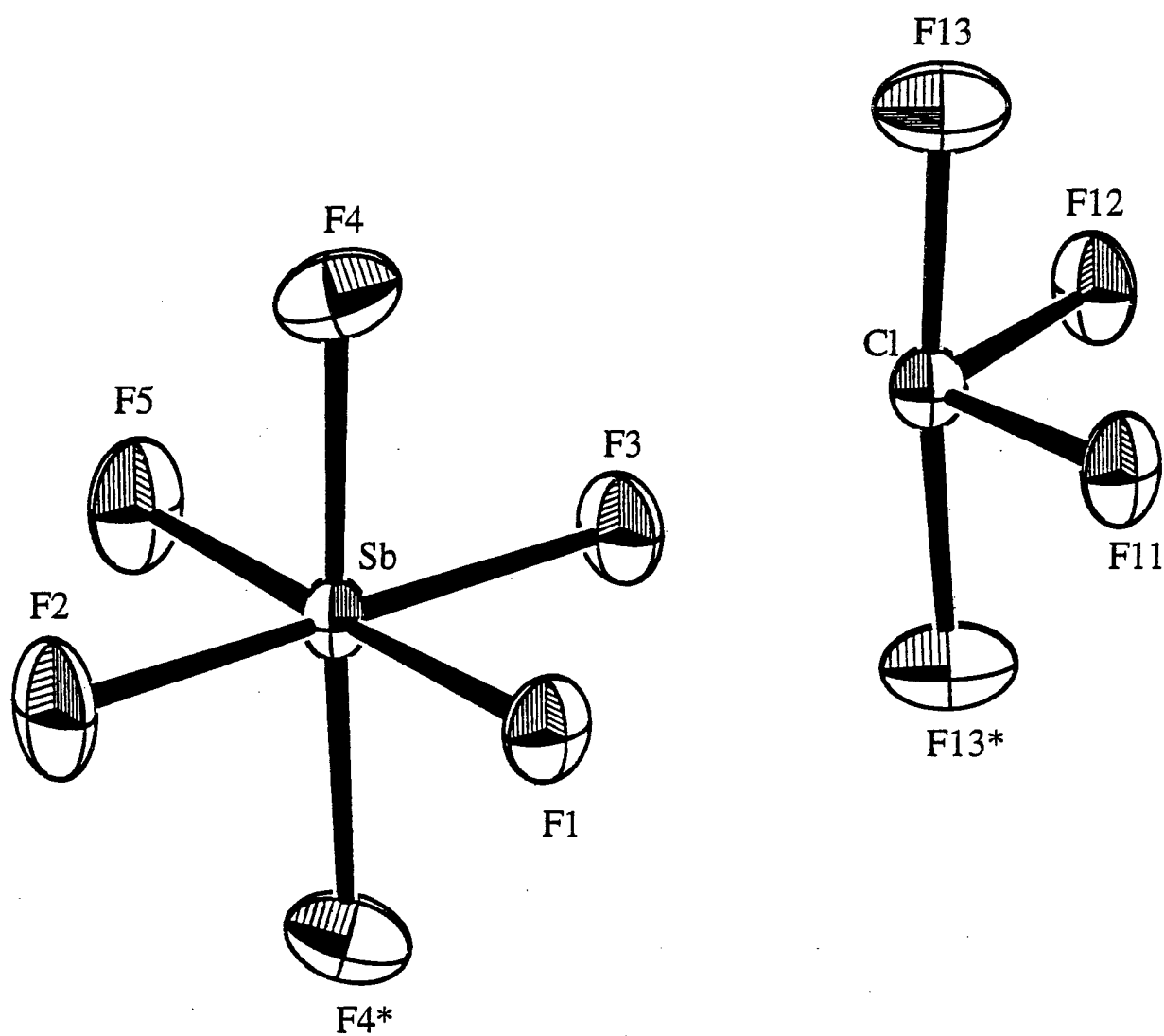


Figure 1. Ortep Plot of $\text{ClF}_4^+\text{SbF}_6^-$; thermal ellipsoids are shown at the 50% probability level.

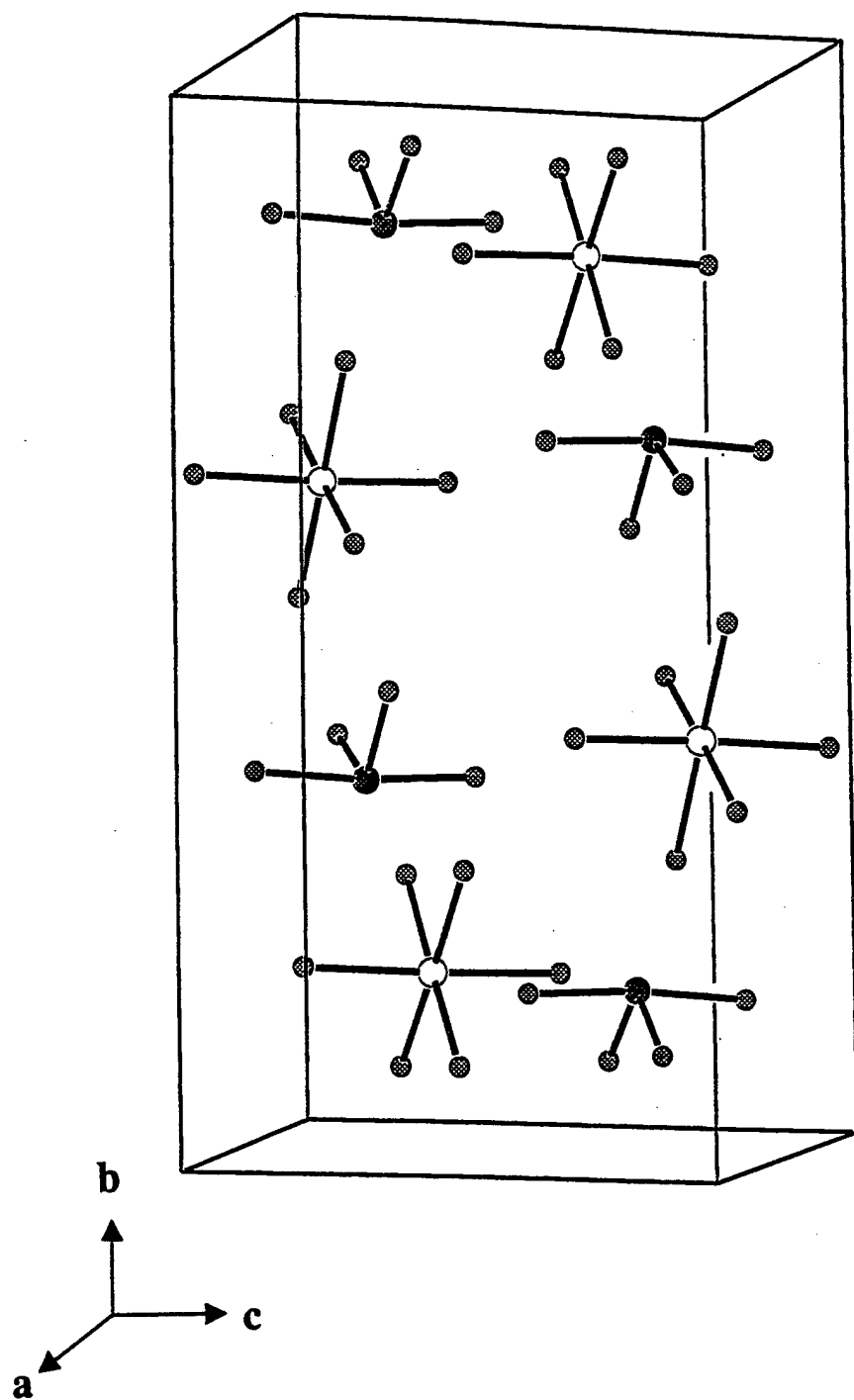


Figure 2. Packing diagram for $\text{ClF}_4^+\text{SbF}_6^-$.

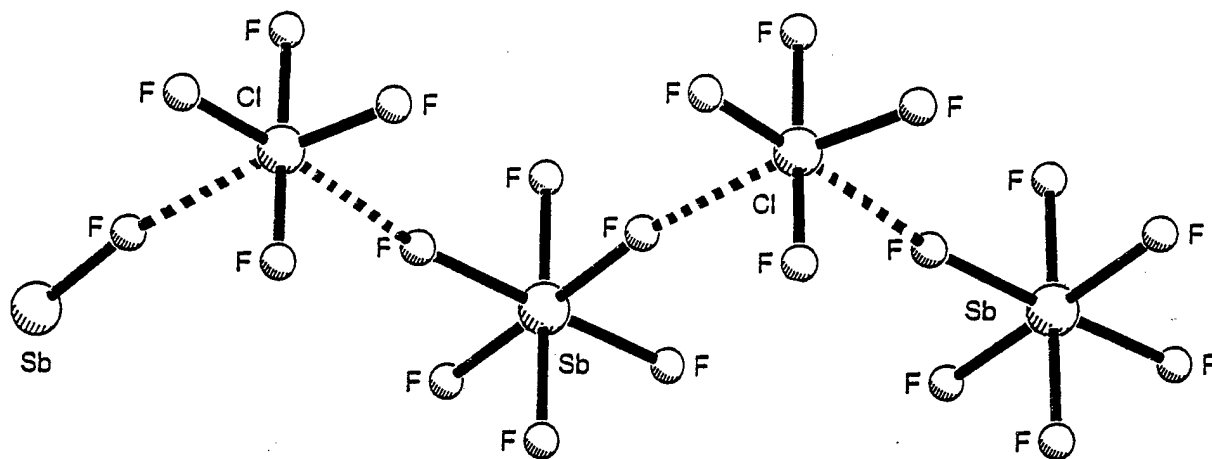


Figure 3. Interionic fluorine bridging in $\text{ClF}_4^+\text{SbF}_6^-$, showing the pseudo-octahedral fluorine environment around chlorine.

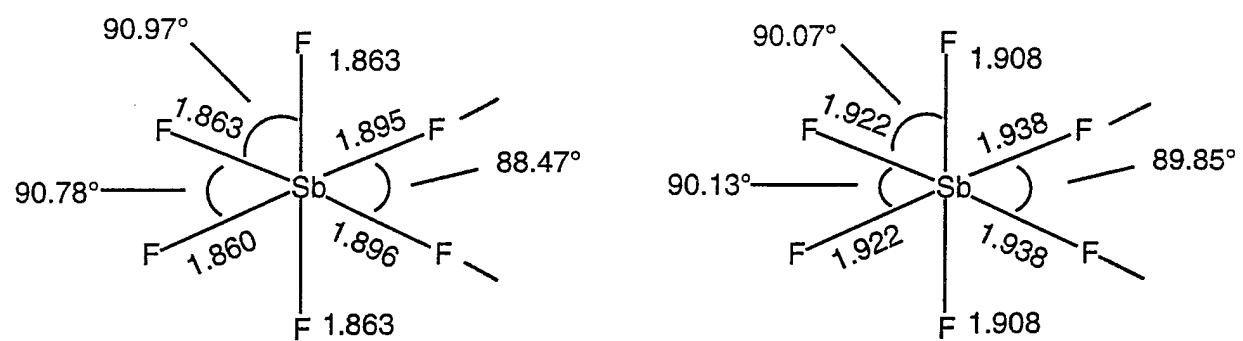


Figure 4. Observed (a) and calculated (b) structures of C_{2v} distorted SbF_6^- .

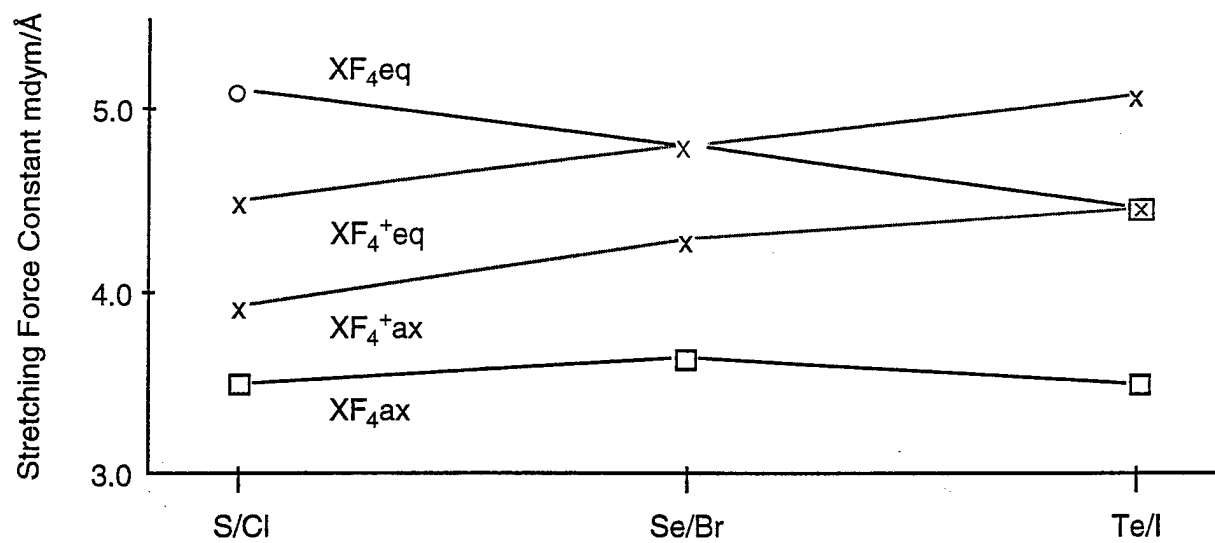


Figure 5. Stretching force constants of the axial and equatorial bonds in the isoelectronic SF_4 , SeF_4 , TeF_4 (solid lines) and ClF_4^+ , BrF_4^+ , IF_4^+ (broken lines) series.